ICAS 2020 SHANGHAI
International Council of the Aeronautical Sciences
32nd Congress of the International Council of the Aeronautical Sciences
Shanghai, China
September 14th-18th, 2020

GEOMETRICAL PARAMETER STUDY OF A HYPERSONIC VERTICAL GAP FLOW

ZHANG Haoyuan[1, 2], ZONG Wengang [3], ZHU Yuanhao [3], GUI Yewei[2], & QIU Bo[1, 2]

[1] State Key Laboratory of Aerodynamics, Mianyang 621000, China
[2] Computational Aerodynamics Institute, CARDC, Mianyang 621000, China
[3] College of Chemical Engineering, Sichuan University, Chengdu 610065, China

Abstract

A numerical study on a hypersonic vertical gap flow is presented. Based on the simplified model of the wing-leading-edge gap from a previous study, where the basic characteristics of the flow structure and wall heat flux distribution were analyzed, a series of gap models with different depths and widths has been established. The influence of the geometrical parameters to the vortex structure and aerodynamic heating were investigated. The results suggest that, at a given gap-depth, with the increase of the gap-width, the number of vortices in the gap will go up from one pair to three pairs, which would lead to an increase of the number of the “bright belt” of wall heat flux on the sidewall of the gap from one to two. The comparison of the results from gap models at the same width (of 5mm) but different depths suggests that the increase of gap depth has a less impact on the variation of vortex structure seen in the cases with different gap widths. A deeper gap, however, would lead to faster fluid entering the gap, resulting in a rapid increase of the peak values of wall heat flux on the sidewall of the gap.

Keywords: Hypersonic, Vertical gap, Aerodynamic heating, Vortex structure

1. Introduction

The thermal protection system (TPS) is essential and vital for hypersonic long-endurance vehicles. These vehicles, especially at the nose and the wing-leading-edge, usually have very complex thermal protection system due to the serious aerodynamic heating. Gaps, between the protection elements, are introduced to absorb thermal expansion and reduce thermal stress. These gaps, however, may introduce a significant increase of the local aerothermal loads, which could cause a serious damage to the whole TPS, or even the vehicle itself. A number of studies [1-5] have been carried out to investigate the impact of the transverse gaps on the vehicle surface to the flow structure and aerodynamic heating. While, besides these transverse gap flows, there is another type of gap flows, the vertical gap flows, which could also cause severe increase of aerothermal loads and potential damage to the vehicles. For the vertical gap flows, as the high temperature and high-speed flow will directly run into the gap, the heating loads could be much higher than those seen in the transverse gap cases. Nevertheless, the studies on such vertical gap flows are much less than those for the transverse gap flows.

In a previous study of such vertical gap flows, Zhang et. al [6] proposed a simplified model of the wing-leading-edge gap and used it to investigate the basic flow structure and characteristic of the aerodynamic heating at a Mach number of 7. Moreover, they found that the vortices have a direct impact on the distribution of the wall heat flux along the sidewall of the gap, and the reattached flow induced by the vortices leads to a local peak belt with a maximum value more than twice that at the stagnation line of the leading-edge. In this paper, we focus on the influence of the geometrical parameters of the gap on the flow structure and aerodynamic heating. To pursue this aim, we designed a serious of vertical gap models based on the Zhang et. al [6] vertical gap model and studied

the gap flows at a Mach number of 7.

2. Vertical Gap Models

The vertical gap model in the previous study of Zhang et al [6] is shown in Figure 1, where the radius of the leading-edge (half circle) is 80mm and the width and depth of the gap are 5mm and 10 mm, respectively. It is not different to find that for such a model, not only the geometrical parameters of the gap but also the geometrical parameter of the leading-edge model itself, such as the radius of the "half circle", can all have a certain impact on the flow structure around the gap. This leading-edge-gap model is a simplified model of the gap region of the wind-leading-edge of a hypersonic vehicle and, in reality, the geometrical parameters of the leading-edge are often compliance to the overall design of the vehicle itself. Therefore, for a given leading-edge model, the variation of the gap structure is mainly determined by the gap itself. Based on this, two sets of variations of the vertical gap models were proposed. They are the gap models at a given width with different depth and the ones at a given depth with different width. Figure 2 presents the schematic of models at a given width of 10 mm, and the geometrical parameters of all of the three sets of gap models are listed in Table 1.

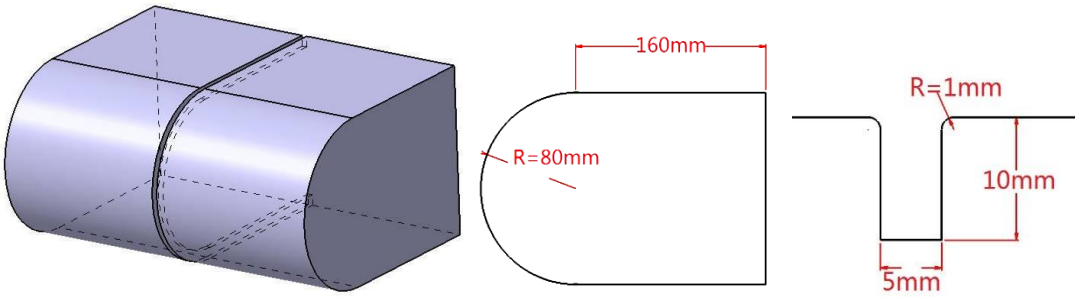

Figure 1 - The original simplified model of the wing leading-edge gap (from Zhang et. al [6])

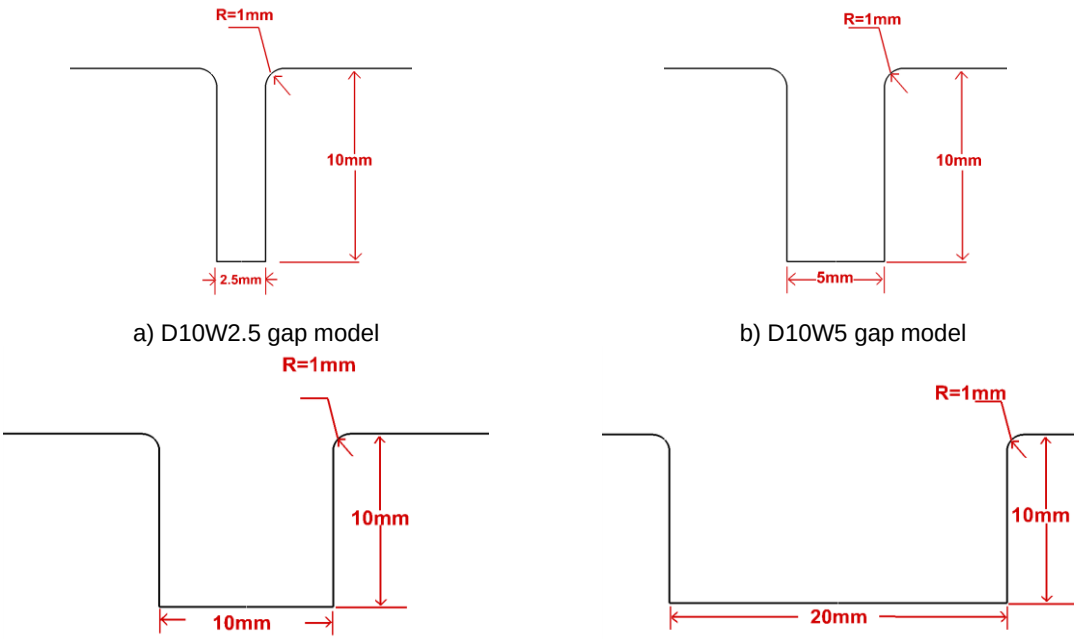

a) D10W2.5 gap model

b) D10W5 gap model

c) D10W2.5 gap model

d) D10W5 gap model

Figure 2 - Geometrical parameters of the 10mm depth gap models

Table 1 Geometrical parameters of the gap models employed.

Group	Gap Model	Depth/mm	Width/mm
Set 1	D10W2.5	10	2.5
Set 1	D10W5	10	5
Set 1	D10W10	10	10
Set 1	D10W20	10	20
Set 2	D5W5	5	5
Set 2	D10W5	10	5
Set 2	D20W5	20	5

3. Numerical Method

The Navier-Stokes equations for compressible flows are solved with the Finite Volume Method (FVM) via an in-house CFD platform, which is a three-dimensional, multi-structured-block, fully implicit code. This solver employs flux-vector-splitting (FVS) schemes, such as the van Leer and AUSMPW+ schemes, to discretize the inviscid fluxes. The Monotonic Upwind Scheme for Conservation Laws (MUSCL) approach with the van Albada limiter, developed by Anderson et. al [7], is used for the interface interpolations of the primitive variables to provide high-order accuracy in space. The central-differencing scheme is employed for the viscous fluxes. The lower-upper symmetric Gauss-Seidel (LU-SGS) [8] implicit scheme is used for the time advancing, and the local time marching method is employed to accelerate convergence to steady state. In the present study, the van Leer FVS scheme with the total enthalpy preserving modification proposed by Hänel et al. [9] is selected to define the inviscid fluxes with the consideration of the balance of accuracy and stability.

4. Case Set-up

The freestream conditions are *Ma*=7, *Re*/m=1.2×10^6 and T_∞=236.5K. The working medium, air, is treated as a perfect gas, and the flow is assumed to be fully laminar. The freestream values are set to the inlet boundary and the extrapolation condition is applied for all variables at the outlet boundary. At the wall, the no-slip condition is applied for velocity, with wall temperature, T_{wall}, fixed to 300K and zero gradient for pressure. The numerical simulations have been performed using multi-blocked-structured grids. Figure 3 presents the computational grids in the gap region of the models with gap-depth of 10mm. The grid in the gap region for the D10W5 gap model is 116×112 cells (D*W), maintaining the cell Reynolds number, the Reynolds number based on the height of the first cell off the wall, equals 8 and at least 20 cells inside the boundary layer. This grid is also selected to be the base of the grids for the D10W10 and D10W20 gap models, where the near wall region remains the same as the D10W5 grid. The grid for the D10W2.5 gap model shares the same mesh topology, as well as the grid distribution in the depth direction and the size of the first cell off the wall, as the D10W5 model with the only exception of the cell number in the width direction, which is 88. The whole "T"-shape area of the computational mesh above the model surface is high enough to cover the boundary layer developing from the stagnation line of the gap model. The grid of the outer flow field is shown in Figure 4, where the distribution of the grid points near the bowl shock wave has been optimized with the shock wave shape obtained from a previous calculation. Since the flow field is symmetric (the angle of attack of the freestream is 0°), only the upper half of the flow domain is used for the numerical simulations, and the total cell numbers of these for grid is listed in Table 2. The grid used for the rest of the gap models with different widths and depths are generated in a similar way as the models with gap-depth of 10mm.

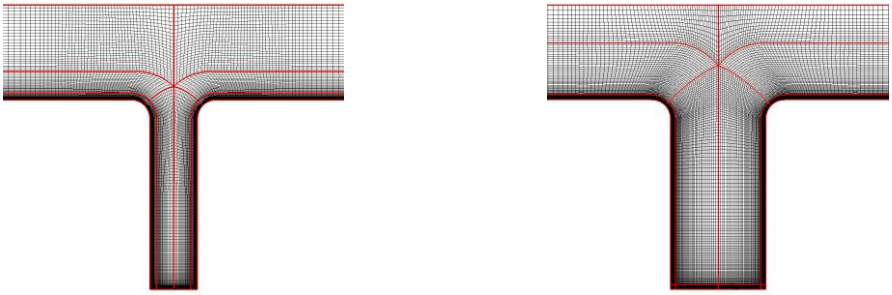

a) D10W2.5 gap model

b) D10W5 gap model

c) D10W10 gap model

d) D10W20 gap model

Figure 3 – Computational grids for the 10mm depth gap models in the gap region

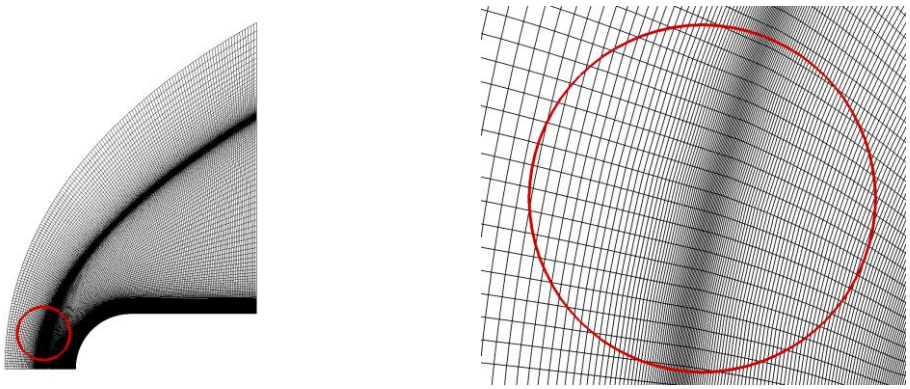

a) Out flow field mesh

b) shock matching and refinement

Figure 4 – Computational grids for the 10mm deep gap models in outer flow field

Table 2 Cell numbers of the computational grid used for the 10mm deep gap models

Gap Model	D10W2.5	D10W5	D10W10	D10W20
Cell Number	4,508,928	5,381,408	6,165,728	7,732,368

5. Results and Discussion

5.1 Validation Case

The case tested here is a simple example to show the performance of this in-house CFD solver on the prediction of aerodynamic heating in hypersonic laminar flows. The experimental case of hypersonic flow over a 2D cylinder from Wieting [10] is selected here, since this configure is similar to the leading-edge model in this study without the gap. The inflow conditions are *Ma* = 8.03, T_∞ = 124.94*K*, T_{wall} = 294.44K and *Re*/m = 1.835×10^5. The reference length is the radius of the cylinder, which is set to be 1 meter in the present simulation. The computational grid used is 72×120 cells

(shown in Figure 5 (a)) and the cell Reynolds number at the stagnation point is 8. The basic structure of the flow field is shown in Figure 5(b) and Figure 5(c). The pressure and Mach number distribution show that the numerical flow field is smooth, without oscillations, and the shock wave is captured accurately. Figure 6 compares the non-dimensional wall pressure and heat flux along the cylinder surface with the experimental data. The value at the stagnation point is used to normalize the pressure and heat flux. The predicted wall pressure and heat flux are in good agreement with the measured data. The predicted wall heat flux at the stagnation point is 19.15kW/m^2, which is also close to the theoretical result from the Fay-Riddell formula, 17.46kW/m^2. The comparisons of the wall pressure and heat flux shows that this solver can give a reasonable prediction of both the wall pressure and heat flux and, therefore, be used with confidence to carry out further simulations of such hypersonic laminar flows.

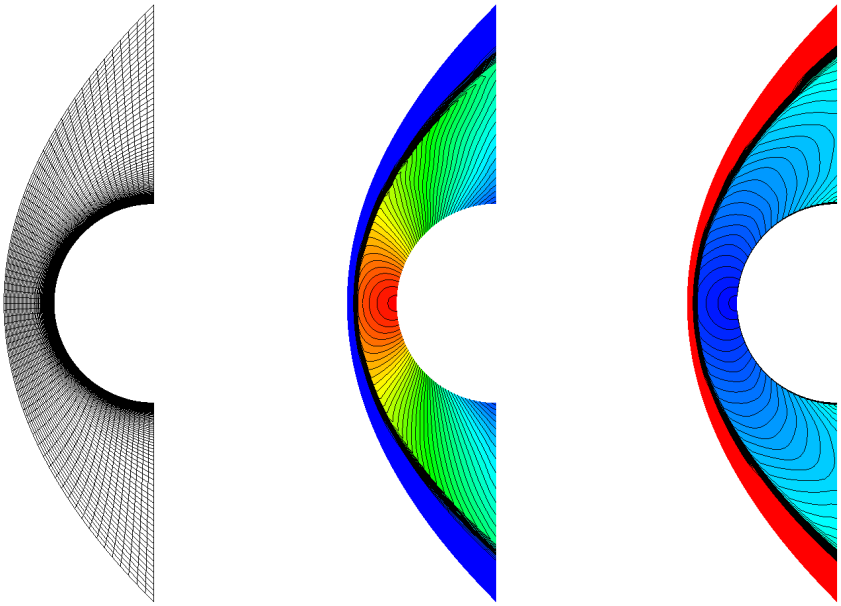

a) Computational grid b) Contours of pressure c) Contours of Mach number

Figure 5 – Computational grids and Contours of pressure and Mach number for the 2D hypersonic cylinder case

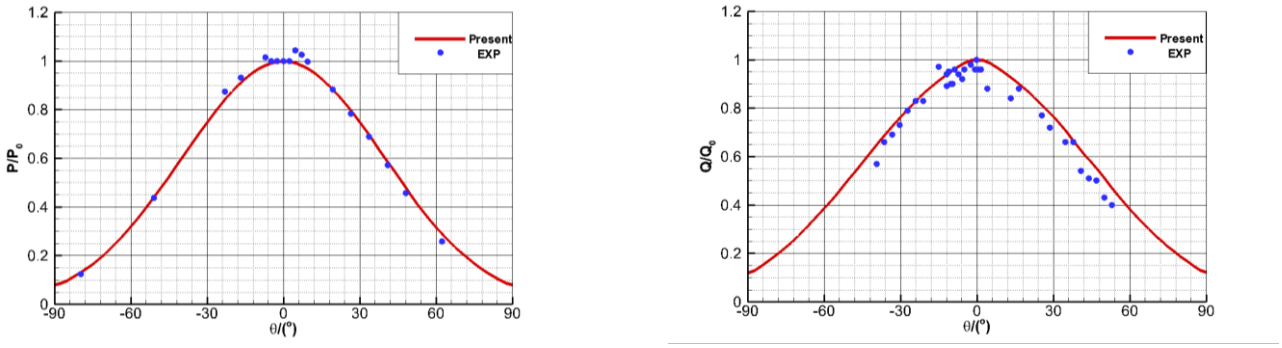

a) Wall pressure b) Wall heat flux

Figure 6 – Comparison of wall pressure and heat flux of the 2D hypersonic cylinder case

5.2 Impact of the gap width on flow structure and wall heat flux

The outline of the gap model is presented in Figure 7 and the P1 section is along the stagnation line of the leading-edge and parallel to the inflow direction. Since the wall, inside and outside the gap, around P1 section faces the most severe aerodynamic heating on the whole gap model surface, this

section is chosen to carry out the analysis of the predicted flow field and wall heat flux distribution in this work. The 2D streamlines, superimposed on contours of stream-wise velocity, in the P1 section, of the four gap models, the D10W2.5 model, the D10W5 model, the D10W10 model and the D10W20 model, are compared in Figure 8. Only one pair of vortices appears near the bottom of the gap for the narrowest gap model, the D10W2.5 model. The number of vortices increases to two pairs for the D10W5 model, where one major pair of vortices is located in the middle of the gap with another pair of smaller vortices lying near the upper half of the gap. For the two wider gap models, the D10W10 model and the D10W20 model, three major pairs of vortices exit near the upper half of the sidewall of the gap. Both the speeds of the flow entering the gap and the reverse flow induced by the bottom surface of the gap increase as the width of the gap enlarged, which indicates that the aerodynamic heating caused by the these vortices may become more serious as well.

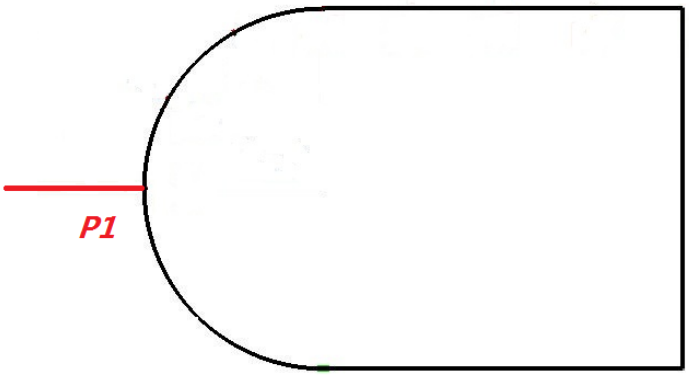

Figure 7 – Outline of the gap model and the position of the P1 section

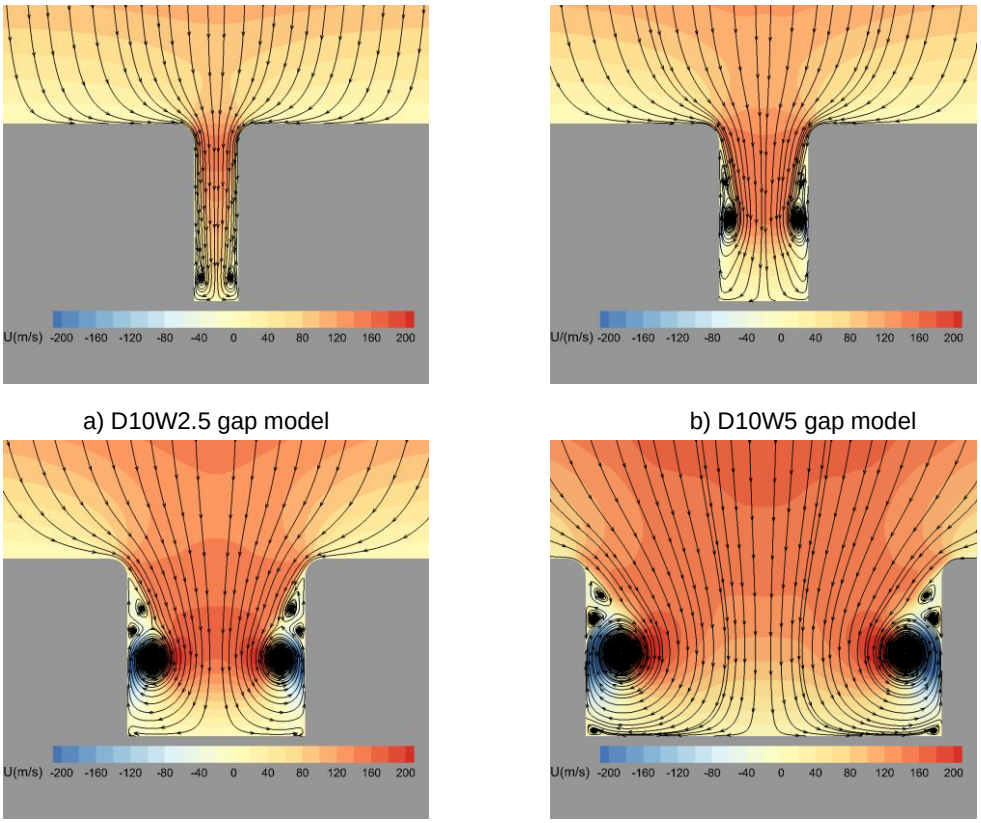

a) D10W2.5 gap model

b) D10W5 gap model

c) D10W10 gap model

d) D10W20 gap model

Figure 8 – Comparisons of the 2D streamlines and velocity in the P1 section for gap models at the same depth of 10mm

The contours of the predicted wall heat flux, as well as the 2D streamlines in the P1 section, in the neighborhood of the leading-edge in the gap, for the four gap models, are presented in Figure 9 (only half of the flow field is presented here due to its symmetry). Seen from these figures, there is only one “bright belt” of the local peaks of wall heat flux on the sidewall of the gap for the D10W2.5 and D10W5 models, where the main difference is that the location of the “bright belt” for the D10W2.5 is rather close to the bottom of the gap while the one for the D10W5 model is near the middle of the sidewall of the gap. The three pairs of vortices induced by the D10W10 and D10W20 gaps result in two local peak-belts of wall heat flux along the sidewall of the gap. The peaks of theses local peak-belts of wall heat flux for the four gap models, as well as the peak values at the leading-edge without gap effect, are listed in Table 3. The predicted peaks of the local peak-belts on the sidewall of the gap models are more than twice of that at the leading-edge, except for the narrowest model, the D10W2.5 model, where the predicted peak value is approximately 50% higher.

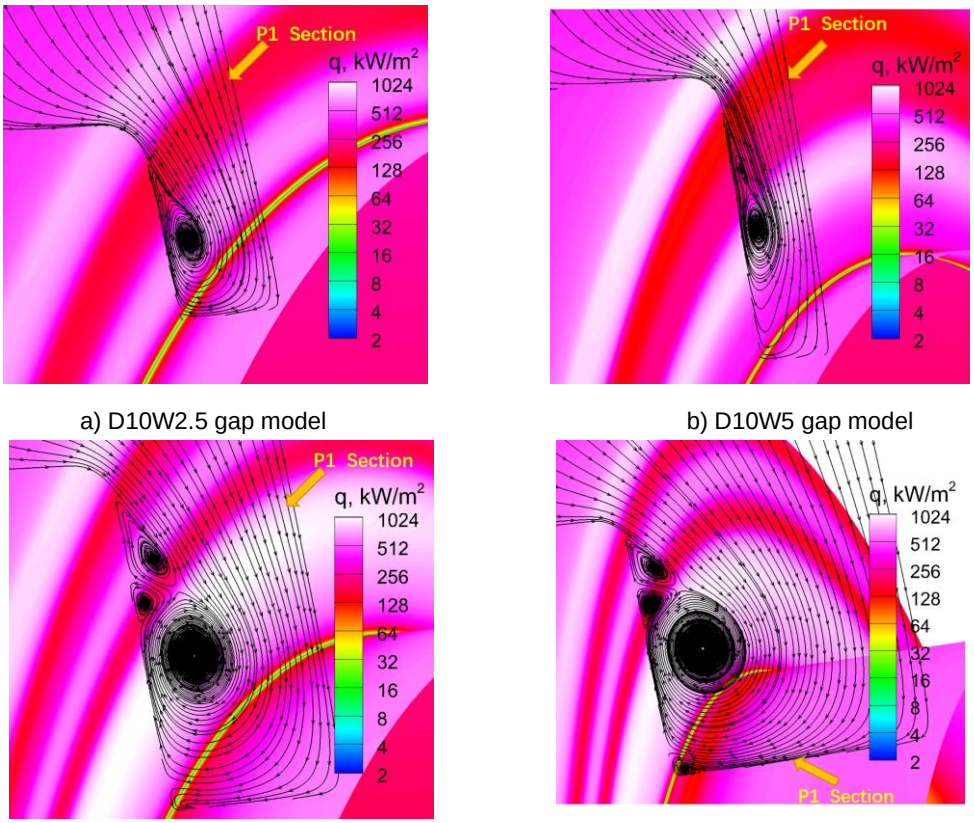

a) D10W2.5 gap model

b) D10W5 gap model

c) D10W10 gap model

d) D10W20 gap model

Figure 9 – Comparisons of the wall heat flux around the leading-edge for gap models at the same depth of 10mm

Table 3 Peaks of wall heat flux on the leading-edge of the gap models at the same depth of 10mm, inside and outside the gap

Gap Model/Leading-edge outside the gap	D10W2.5	D10W5	D10W10	D10W20	Leading-edge outside the gap
Peak of wall heat flux (kW/m^2)	619.95	866.44	1090.48	1025.63	398.53

5.3 Impact of the gap depth on flow structure and wall heat flux

Figure 10 compares the 2D streamlines, together with the contours of stream-wise velocity, in the P1 section, with the use of the three gap model with the same gap width, the D5W5 model, the D10W5 model and the D20W5 model. For the two deeper model, the D10W5 model and the D20W5 model,

two pairs of vortices can be seen in the gap, while for the shallowest model, the D5W5 model, only one pair of vortices exits. The locations of the vortices in the two deeper model, however, are different, where the major pair of vortices in the D10W5 model lies in the middle section of the gap, but the ones in the D20W5 model are quite close to the bottom of the gap. It can also be found from the contours of stream-wise velocity that the speed of the fluid running into the gap increases with the gap depth, which might consequently cause greater aerodynamic heating.

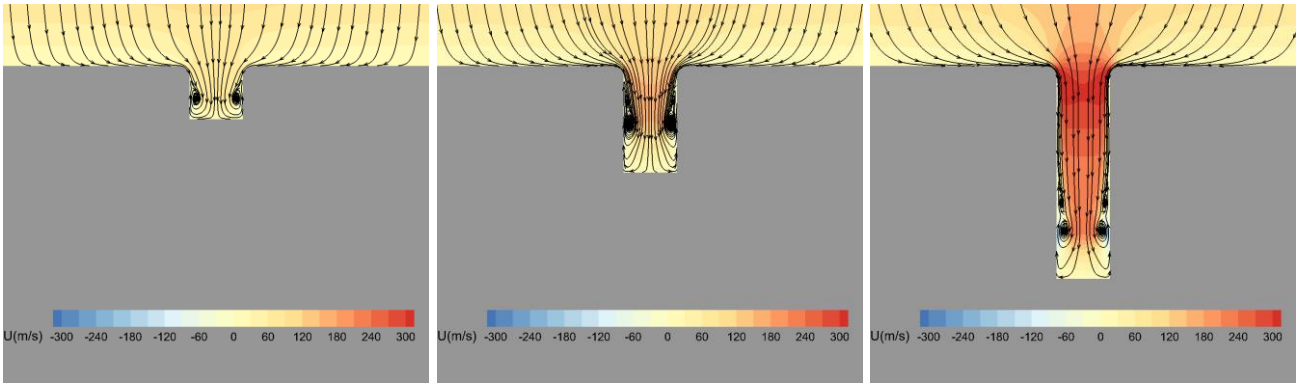

a) D5W5 gap model b) D10W5 gap model c) D20W5 gap model

Figure 10 – Comparisons of the 2D streamlines and velocity in the P1 section for gap models at the same width of 5mm

The predicted wall heat flux and the 2D streamlines in the P1 section (only half of the flow field is presented here due to its symmetry) for the three gap models at the same gap width of 5mm are compared in Figure 11. It can be found that, on the sidewall of each gap model, there is one major “bright belt” of local peaks of wall heat flux, introduced by the reattachment of the major vortex near the sidewall. Note that for the deepest gap, the D20W5 model, another local peak belt of wall heat flux appears on the sidewall due to the reattachment of the smaller vortex above the sidewall and its peak values are much lower than those of the “bright belt”. The peaks of wall heat flux along the leading-edge, inside and outside the gap, are listed in Table 4. As expected, as the gap goes deeper, the peak value of the wall heat flux on the sidewall of the gap increases rapidly. The peak of the deepest gap model, the D20W5 model, is over 2.8 times of that at the leading-edge outside the gap, and almost 70% higher than that of the D5W5 model.

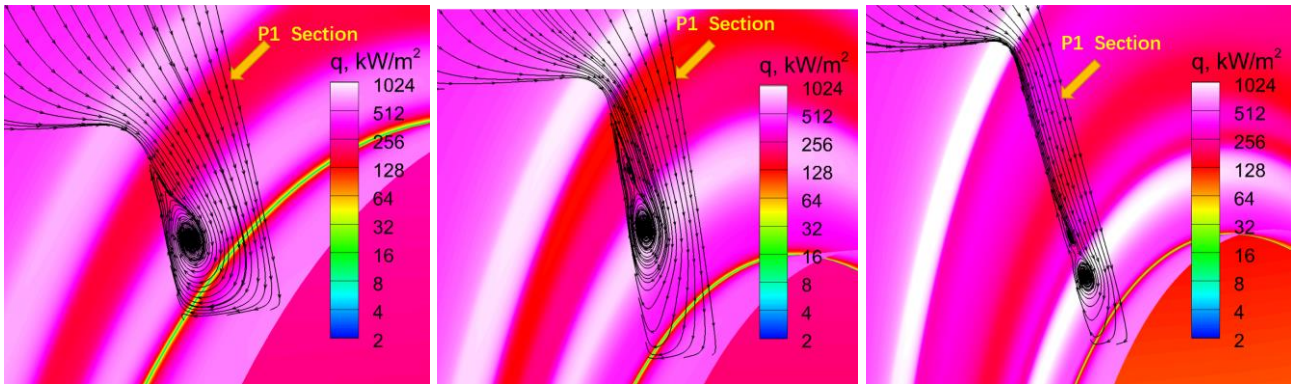

a) D5W5 gap model b) D10W5 gap model c) D20W5 gap model

Figure 11 – Comparisons of the wall heat flux around the leading-edge for gap models at the same width of 5mm

Table 4 Peaks of wall heat flux on the leading-edge of the gap models at the same width of 5mm, inside and outside the gap

Gap Model/Leading-edge without gap	D5W5	D10W5	D20W5	Leading-edge without gap
Peak of wall heat flux (kW/m^2)	667.02	866.44	1126.09	398.53

6. Conclusions

The influence of the geometrical parameters on the flow structure and aerodynamic heating of a hypersonic vertical gap flow has been investigated numerically. The numerical results showed that as the gap-width increases at a given gap-depth (of 10mm), the vortex structure becomes more complex, there the most significant change is the number of vortices. In particular, only one major vortex appears near the bottom of the 2.5mm-width gap model, while one major vortex accompanied with a second “flat” vortex presents around the middle of the 5.0mm-width gap model. In both of these two cases, there is only one “bright-belt” of local peaks of the wall heat flux on the sidewall of the gap, with the main difference lies in the location and the magnitude of the peak values. The 10mm-width and 20mm-width gaps would both induce three vortices above the sidewall of the gap and result in two local peak-belts of wall heat flux. The impact of the gap depth at a given gap-width (of 5mm) on the vortex structure and wall heat flux has also been investigated. The number of vortices would increase from one pair for the 5mm deep gap to two pairs for the 10mm and 20mm gap. Unlike the change of the “bright -belt” caused by the gap-width, there would be one major local peak belt on the sidewall of the gap for the three gap models tested. From the comparisons of the numerical results of the two sets of gap models, it can be concluded that the actual structure of the vortices induced by the gap, at a certain inflow condition, mainly depends on the width of the gap.

7. Contact Author Email Address

Mailto: wgzong@scu.edu.cn

8. Copyright Statement

Acknowledgements

The authors gratefully acknowledge the financial support of the National Key Research and Development Plan of China through project No. 2019YFA0405202 and the National Natural Science Foundation of China (Grant Numbers: 11802324 and 12002361).

References

[1] Everhart J L. Supersonic/Hypersonic Laminar Heating Correlations for Rectangular and Impact- Induced Open and Closed Cavities [J]. *Journal of Spacecraft & Rocket*, Vol 46, No. 3, pp 545-560, 1971.

[2] Tang G. Experimental investigation of heat transfer distributions in a deep gap [J]. *Experiments and Measurements in Fluid Mechanics*. 2000, 14(4):1-6. (in Chinese)

[3] Qiu B, Zhang H, Guo Y, et. al. Numerical investigation for vortexes and aerodynamic heating environment on transverse gap on hypersonic vehicle surface [J]. *Acta Aeronautica et Astronautica Sinica*, Vol. 36, No. 11, pp 3515-3521,2015. (in Chinese)

[4] Qiu B, Guo Y, Zhang H, et. al. Free stream parameters' effects on vortexes and aerodynamic heating environment in thermal protection tile transverse gaps [J]. *Acta Aeronautica et Astronautica Sinica*, Vol. 37, No. 3, pp 761-770,2016. (in Chinese)

[5] Qiu B, Zhang H, Shi Y, et. al. Numerical investigation of geometric parameters effects on transverse gaps on hypersonic vehicle [C]. *21st AIAA International Space Planes and Hypersonics Technologies Conference*, Xiamen China, March 6, 2017 – March 9, 2017.

[6] Zhang H, Zong W, and Gui Y. Numerical investigation of flow in leading-edge gap of hypersonic vehicle [J]. *Journal of Astronautics.* Vol. 35, No. 8, pp 893-900, 2014 (in Chinese)

[7] Anderson W K, Thomas J L, Van Leer, B. Comparison of finite volume Flux Vector Splittings for the Euler equation [J], *AIAA Journal*, Vol 24, No. 9, pp 1453-1460, 1986

[8] Yoon S. LU-SGS implicit algorithm for three-dimensional incompressible Navier-Stokes equations with source term. AIAA-89-1984-CP, *9th AIAA CFD Conference*,1989

[9] Hänel D, Schwane R, and Seider G. On the accuracy of upwind schemes for the solution of the Navier-Stokes equations, *AIAA paper*, No. 1105, 1987

[10]Wieting A R. Experimental study of shokc wave interference heating on a cylindrical leading edge. *NASA TM*, No. 100484,1987